Surface Domain Configuration of Nd-Fe-B Sintered Magnets Influenced by Underneath Magnetization

M. Takezawa, Y. Ichihara, Y. Morimoto, and J. Yamasaki

Dept. of Applied Science for Integrated System Eng., Faculty of Eng., Kyushu Institute of Technol., Kitakyushu 804-8550, Japan

The influence of underneath magnetization of Nd-Fe-B sintered magnets on surface domain configurations was investigated using a Kerr microscope by cutting the magnets at an angle to the c-axis. When the angle formed by the surface and the c-axis is larger than 30 degrees, the observed domain configurations change to maze patterns because of an increase in the demagnetizing field at the surface. In contrast, when the cutting angle is 10 degrees, residual magnetization increases with the applied field. It was found that at a cutting angle of 10 degrees, the underneath domain configurations can be indirectly observed through the surface by propagation of magnetic flux from the underneath grains.

Index Terms—**Kerr effect microscopy, magnetic domain observation, Nd-Fe-B sintered magnet, sample preparation technique.**

I. Introduction

Nd-Fe-B SINTERED magnets have been widely used for motor applications because of their large energy product [1]. It is well known that microfabrication of these magnets by polishing decreases their coercive force and influences the driving characteristics of micromotors [2]. The important role of the Nd-rich phase in grain boundaries in obtaining high coercive force has been reported [3]. Therefore, domain observations around grain boundaries would be useful in solving durability problems involved in microfabrication [4], [5]. However, it is difficult to observe the underneath domain configurations in Nd-Fe-B sintered magnets using a Kerr microscope, because the observable domain configurations on the surface of polished grains losing coercivity can be completely different from the underneath domain configurations [6]. This paper proposes a sample preparation technique for observing the underneath domain configurations by cutting at an angle to the c-axis of Nd-Fe-B magnets, and reports the relationship between the domain configurations and the cutting angle.

II. Experiment

A Kerr microscope was used to view the magnetic domains of Nd-Fe-B sintered magnets used in a voice coil motor. The magnets were cut in samples 3.0 mm thick, 11.0 mm long, and 7.0 mm wide, and the sample surfaces were polished to observe the domain configuration clearly. In addition, a thin SiO film was deposited as an oxidation resistant coating on the magnet surfaces by vacuum evaporation, and its thickness was controlled to $\lambda/4$ to serve as an antireflection coating. The wavelength of the light used for observation was $\lambda = 546$ nm.

Because Nd-rich grain boundary layers are removed by polishing, grains around the polished surface lose their coercivity. Therefore, the surface domain configurations parallel to the c-axis could be different from the underneath domain configurations, as shown in Fig. 1(a). In contrast, when the observed surface is the c-plane (perpendicular to the c-axis), the surface domain configurations are affected by the underneath domain configurations because of magnetostatic coupling between the magnetization in the damaged grains and that in the underneath grains, as shown in Fig. 1(b). However, the surface domain configurations could be different from the underneath domain configurations because a large demagnetizing field is present at the surface. Moreover, it is difficult to apply a magnetic field to a magnet along the c-axis during domain observation as it is the difficult to position the microscope and the electromagnet.

In this study, magnets were cut at an angle to the c-axis to obtain information of the underneath domain configuration through the surface using a Kerr microscope, as shown in Fig. 1(c). The angles between the observed surface and the c-axis were 0, 10, 30, and 45 degrees. For a cutting angle of 0 degrees, the longitudinal direction of the magnet was along the c-axis of the magnet. A dc field was applied along the longitudinal direction to explore the domain configuration and the magnetization process. First, a magnetic field was gradually increased from 0 to 2.0 kOe, then that field was removed. Next, a magnetic field up to 4.0 kOe was applied and then removed. This procedure was repeated up to 16.0 kOe in 2.0 kOe increments of field strength for each application.

III. Results and Discussion

Fig. 2 shows the domain images of the magnet at a cutting angle of 0 degrees when a dc field was applied along the longitudinal direction. In the images, bright and dark domains have magnetizations pointing rightward and leftward, respectively. Stripe domain patterns in the longitudinal direction were observed, and the stripe patterns crossed a few grains in a demagnetization state, as shown in Fig. 2(a). When the dc field was increased up to 2.0 kOe, domain walls moved and the area of the bright domains increased, as shown in Fig. 2(b). When the field was removed, the area of the dark domains increased and the domain configuration returned to that in the demagnetization state, as shown in Fig. 2(c). When the dc field reached 4.0 kOe, the domain configuration changed to a saturation state at the surface, as shown in Fig. 2(d). However, when the field was removed, the domain configuration returned to a multidomain configuration, as shown in Fig. 2(e). A single domain configuration in a remanent state was obtained after applying a dc field of 10.0 kOe, as shown in Fig. 2(f).

Manuscript received March 06, 2009. Current version published September 18, 2009. Corresponding author: M. Takezawa (e-mail: take@ele.kyutech.ac.jp).

Digital Object Identifier 10.1109/TMAG.2009.2021772

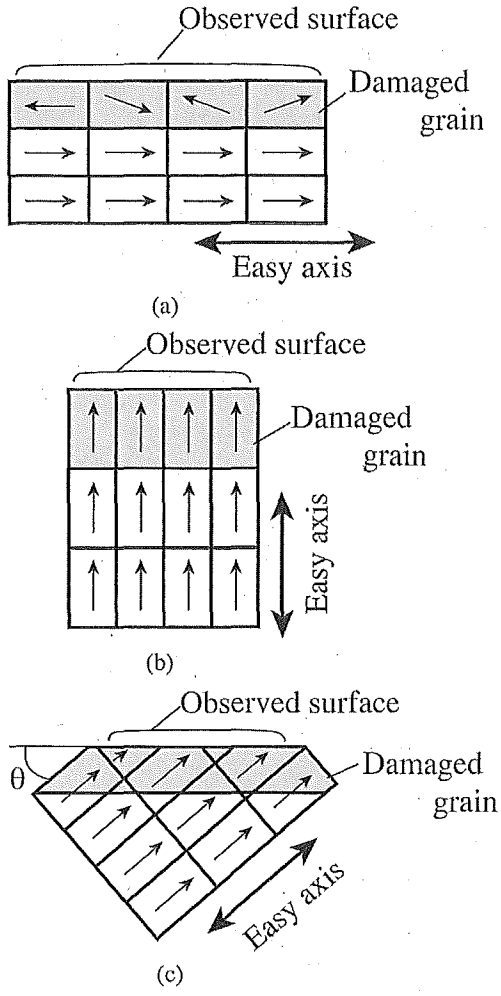

Fig. 1. Observed surface and magnetostatic interaction between surface magnetization and underneath magnetization in Nd-Fe-B sintered magnets: (a) cutting angle, $\theta = 0$, (b) $\theta = 90$ degrees, and (c) $0 < \theta < 90$ degrees.

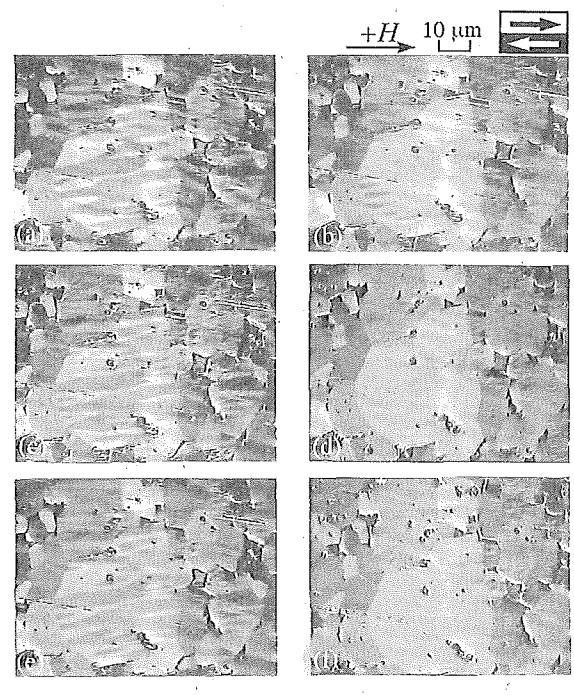

Fig. 2. Domain images of the magnet at a cutting angle of 0 degrees: (a) demagnetization state, (b) $H = 2.0$ kOe, (c) remanent state after applying 2.0 kOe, (d) $H = 4.0$ kOe, (e) remanent state after applying 4.0 kOe, and (f) remanent state after applying 10.0 kOe.

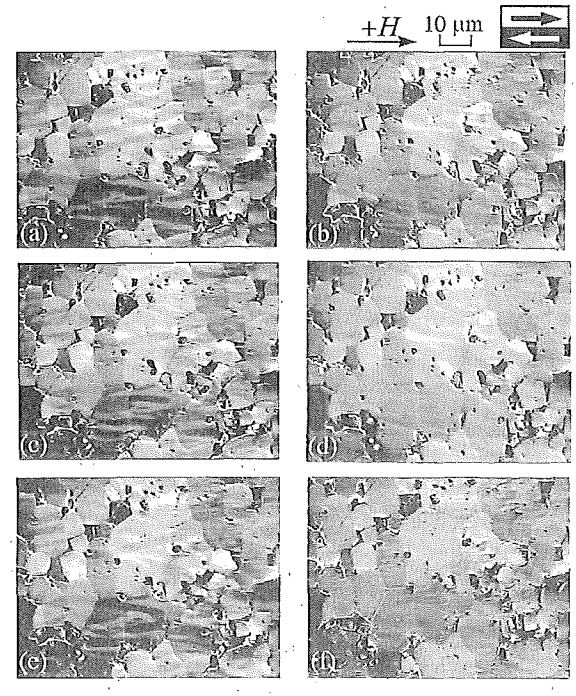

Fig. 3. Domain images of the magnet at a cutting angle of 10 degrees: (a) demagnetization state, (b) $H = 2.0$ (1.97) kOe, (c) remanent state after applying 2.0 kOe, (d) $H = 4.0$ (3.93) kOe, (e) remanent state after applying 4.0 kOe, and (f) remanent state after applying 10.0 kOe.

Fig. 3 shows the domain images of the magnet at a cutting angle of 10 degrees. The c-axis component of the applied field strength along the longitudinal direction is shown in parentheses in the figure captions. Stripe domain patterns in the longitudinal direction were observed in a demagnetization state, as shown in Fig. 3(a). The domain configuration is similar to that of the magnet at a cutting angle of 0 degrees. When the dc field was increased up to 2.0 kOe, domain walls moved and some grains were saturated, as shown in Fig. 3(b). When the field was removed, the domain configuration returned to a multidomain configuration, as shown in Fig. 3(c). However, the area of the bright domains is larger than that at a cutting angle of 0 degrees. When the dc field reached 4.0 kOe, the domain configuration changed to a saturation state at the surface, as shown in Fig. 3(d). When the field was removed again, the domain configuration returned to the multidomain configuration, as shown in Fig. 3(e). A single domain configuration in a remanent state was obtained after applying a dc field of 10.0 kOe, as shown in Fig. 3(f).

Fig. 4 shows the domain images of the magnet at a cutting angle of 30 degrees. Stripe patterns were bent slightly in the demagnetization state, as shown in Fig. 4(a). When the dc field was increased up to 2.0 kOe, domain walls moved and the area of the bright domains increased, as shown in Fig. 3(b). When the field was removed, the area of the dark domains increased

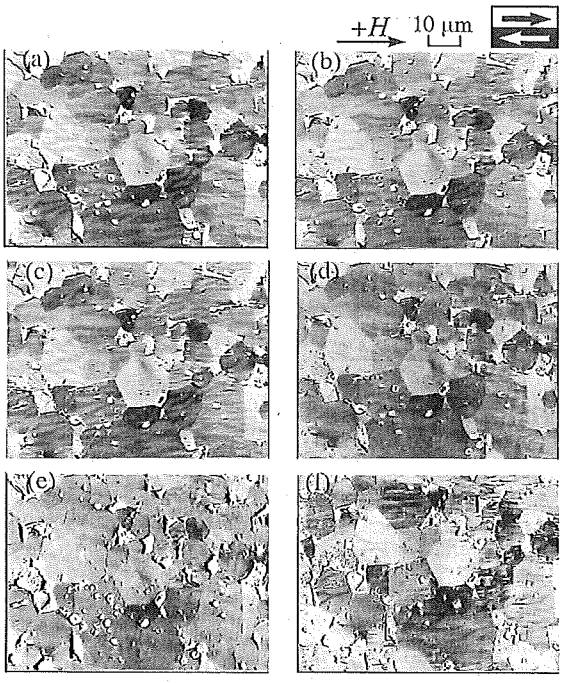

Fig. 4. Domain images of the magnet at a cutting angle of 30 degrees: (a) demagnetization state, (b) $H = 2.0$ (1.73) kOe, (c) remanent state after applying 2.0 kOe, (d) $H = 4.0$ (3.46) kOe, (e) $H = 8.0$ (6.92) kOe, and (f) remanent state after applying 16.0 (13.8) kOe.

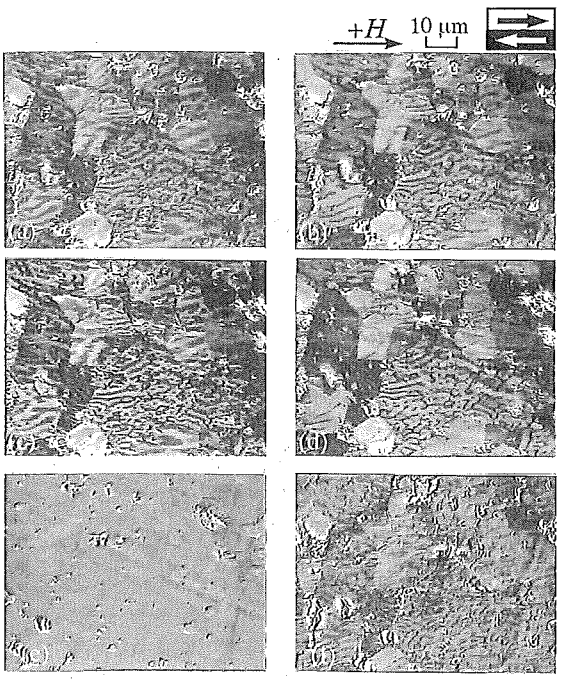

Fig. 5. Domain images of the magnet at a cutting angle of 45 degrees: (a) demagnetization state, (b) $H = 2.0$ (1.41) kOe, (c) remanent state after applying 2.0 kOe, (d) $H = 4.0$ (2.83) kOe, (e) $H = 12.0$ (8.48) kOe, and (f) remanent state after applying 16.0 (11.3) kOe.

and the domain configuration became similar to that in the demagnetization state, as shown in Fig. 3(c). When the dc field increased up to 4.0 kOe, the domain configurations of some grains changed to a saturation state, as shown in Fig. 3(d). When the dc field reached 8.0 kOe, the domain configurations of all grains changed to a saturation state at the surface, as shown in Fig. 3(e). However, the multidomain configurations were observed in a remanent state after applying a dc field of 16.0 kOe. The magnets cut at angles of 0 and 10 degrees show the saturation state at the surface in the remanent state after applying a dc field over 10.0 kOe along the c-axes. However, the multidomain configurations were observed in some grains at a cutting angle of 30 degrees after applying a dc field over 14.0 kOe along the c-axis.

Fig. 5 shows the domain images of the magnet at a cutting angle of 45 degrees. Maze domain configurations were observed in a demagnetization state, as shown in Fig. 5(a). When the dc field was increased up to 2.0 kOe, the area of the bright domains increased, as shown in Fig. 5(b). When the field was removed, the area of dark domains increased and the domain configuration became similar to that in the demagnetization state, as shown in Fig. 5(c). When the dc field was increased up to 4.0 kOe, the domain configurations of some grains changed to a saturation state, as shown in Fig. 5(d). When the dc field reached 12.0 kOe, the domain configuration changed to a saturation state at the surface, as shown in Fig. 5(e). However, the multidomain configurations were observed in a remanent state after applying a dc field of 16.0 kOe.

These domain configurations and magnetization processes at cutting angles of 30 and 45 degrees were different from those at cutting angles 0 and 10 degrees. This change as the cutting angle increased was caused by an increase in the demagnetizing field

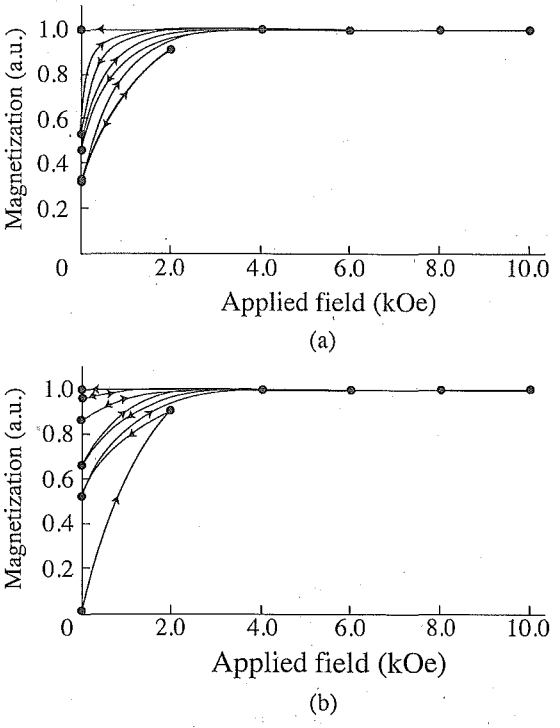

Fig. 6. Magnetization curve processed by Kerr contrast: (a) cutting angle = 0 and (b) cutting angle = 10 degrees.

at the surface. Therefore, the optimum cutting angle is smaller than 30 degrees.

Fig. 6 shows magnetization curves of the magnets at cutting angles of 0 and 10 degrees. The magnetization curve was plotted by processing the brightness of the domain image. The residual magnetization of the magnet at a cutting angle of 0 degrees was

not changed significantly after a field of 2.0 to 6.0 kOe was applied, as shown in Fig. 6(a). However, the residual magnetization at a cutting angle of 10 degrees increased with the applied field, as shown in Fig. 6(b). These data indicate that at a cutting angle of 10 degrees, the underneath domain configurations can be indirectly observed through the surface by propagation of magnetic flux from the underneath grains.

IV. Conclusion

In this study, the influence of underneath magnetizations of Nd-Fe-B sintered magnets on surface domain configurations was investigated using a Kerr microscope by cutting at an angle to the c-axis. When the cutting angle was larger than 30 degrees, the observed domain configurations changed to maze patterns because of an increase in the demagnetizing field at the surface. In contrast, when the cutting angle was 10 degrees, the residual magnetization increased with the applied field and the underneath domain configurations can be indirectly observed through the surface by propagation of magnetic flux from the underneath grains. The optimum cutting angle could enable domain observation including the influence of underneath magnetization. This sample preparation technique solves the problem of deterioration in mechanical fabrication of samples for domain observation using a Kerr microscope.

References

[1] M. Sagawa, S. Hirosawa, H. Yamamoto, Y. Matsuura, and S. Fujimura, "Nd-Fe-B permanent magnet," *Solid State Phys.*, vol. 21, pp. 37–45, 1986, In Japanese.

[2] H. Nakamura, K. Hirota, M. Shimao, T. Minowa, and M. Honshima, "Magnetic properties of extremely small Nd-Fe-B sintered magnets," *IEEE Trans. Magn.*, vol. 41, no. 10, pp. 3844–3846, Oct. 2005.

[3] K. Makita and O. Yamashita, "Phase boundary structure in Nd-Fe-B sintered magnets," *Appl. Phys. Lett.*, vol. 74, pp. 2056–2058, 1999.

[4] D. Li and K. J. Strnat, "Domain behavior in sintered Nd-Fe-B magnets during field-induced and thermal magnetization change," *J. Appl. Phys.*, vol. 57, pp. 4143–4145, 1985.

[5] M. Takezawa, T. Shimada, S. Kondo, S. Mimura, Y. Morimoto, T. Hidaka, and J. Yamasaki, "Domain observation technique for Nd-Fe-B magnet in high magnetic field by image processing using liquid crystal modulator," *J. Appl. Phys.*, vol. 101, pp. 09K106–, 2007.

[6] K. Kobayashi, K. Itoh, D. Shimizu, and K. Hayakawa, "Indirect observation of inner domain structure in $Nd_2Fe_{14}B$ sintered magnets," (in Japanese) *J. Magn. Soc. Jpn.*, vol. 31, pp. 393–397, 2007.